Supplementary material

Mathematical model reveals how regulating the three phases of T-cell response could counteract immune evasion

Running title: *In silico* study of immune competition under immunotherapy

Keywords: T cells; memory; vaccination; theoretical immunology; mathematical modelling

Authors: Tommaso Lorenzi[1,†,*], Rebecca H. Chisholm[2,3,4,†], Matteo Melensi[5], Alexander Lorz[3,4,2], Marcello Delitala[6]

Author's Affiliations: [1] CMLA, ENS Cachan, CNRS, PRES UniverSud, 94235 Cachan Cedex, France; [2] INRIA-Paris-Rocquencourt, MAMBA Team, Domaine de Voluceau, BP105, 78153 Le Chesnay Cedex, France; [3] Sorbonne Universités, UPMC Univ Paris 06, UMR 7598, Laboratoire Jacques-Louis Lions, F-75005, Paris, France; [4] CNRS, UMR 7598, Laboratoire Jacques-Louis Lions, F-75005, Paris, France; [5] Department of Health Sciences, A. Avogadro Università del Piemonte Orientale, 28100 Novara, Italy
[6] Department of Mathematical Sciences, Politecnico di Torino, 10129 Torino, Italy

[†] These primary authors contributed equally to this article

[*] **Corresponding Author:** Tommaso Lorenzi; E-mail: lorenzi@cmla.ens-cachan.fr; Centre de mathématiques et de leurs applications (CMLA), École Normale Supérieure de Cachan, 61, Avenue du Prsident Wilson, 94235 Cachan Cedex, France

Grant Support: This work was supported by the French National Research Agency through the "ANR blanche" project Kibord [ANR-13-BS01-0004]. TL was also

supported by the Fondation Sciences Mathématiques de Paris through a grant overseen by the French National Research Agency [ANR-10-LABX-0098], and by the Hadamard Mathematics Labex, backed by the Fondation Mathématique Jacques Hadamard, through a grant overseen by the French National Research Agency [ANR-11-LABX-0056-LMH].

Disclosure of Potential Conflicts of Interest: The authors disclose no potential conflicts of interest.

Details of the Mathematical Model

We describe the selection dynamics in the cell system through the following coupled integro-differential equations:

$$\frac{\partial}{\partial t} n_C(t,u) = \underbrace{[\alpha_C - \mu_C\, \rho_C(t)] n_C(t,u)}_{\text{proliferation and death of target cells}} - \underbrace{n_C(t,u) \int_0^1 \eta_C(u,v) n_T(t,v) dv,}_{\text{selective action exerted by T cells}} \quad (1)$$

$$\frac{\partial}{\partial t} n_T(t,v) = \underbrace{[1 + c_E(t)] n_T(t,v) \int_0^1 \eta_T(v,u) n_C(t,u) du}_{\text{antigen-driven expansion}} + \underbrace{[1 + c_P(t)]\, \alpha_T\, n_T(t,v)}_{\text{antigen-independent proliferation}} - \underbrace{\frac{\mu_T}{1 + c_M(t)}\, \rho_T(t)\, n_T(t,v).}_{\text{homeostatic regulation}} \quad (2)$$

In the above equations,

$$\eta_T(v,u) := \beta_T\, g(v,u;\gamma,\theta), \qquad g(v,u;\gamma,\theta) := \gamma\, G(u)\, e^{-\frac{(v-u)^2}{\theta}}, \quad (3)$$

and

$$\eta_C(u,v) := \beta_C\, g(u,v;\gamma,\theta), \qquad g(u,v;\gamma,\theta) := \gamma\, G(v)\, e^{-\frac{(u-v)^2}{\theta}}. \tag{4}$$

where $G(\cdot) > 0$ is a normalisation function.

Details of the Numerical Results

Numerical simulations are performed in MATLAB making use of an implicit-explicit finite difference scheme [2] with 600 points on the interval $[0, 1]$. For all simulations, we set the time step $dt = 0.1$.

For T cells, we choose the initial condition

$$n_1(v) := C_1 \quad \forall\, v \in [0;1], \qquad C_1 > 0. \tag{5}$$

For target cells, we make use of the following initial condition

$$n_2(u) := C_2\, e^{-\frac{u^2}{0.001}}, \qquad C_2 > 0. \tag{6}$$

Figure 3(A): Plots of $\rho_T(t)$ (solid line) and $\rho_C(t)$ (dashed line) for $t \in [0; t_f]$ with $t_f := 40$. Simulations are performed with $c_E(t) = c_P(t) = c_M(t) := 0$ for all $t \in [0; t_f]$, $\gamma := 2.5$ and $\theta := 0.1$. The other parameters are defined as in Table 1.

Figure 3(B): Plots of $\rho_T(t)$ (solid line) and $\rho_C(t)$ (dashed line) for $t \in [0; t_f]$ with $t_f := 40$. Simulations are performed with $c_E(t) = c_P(t) = c_M(t) := 0$ for all $t \in [0; t_f]$, $\gamma := 0.4$ and $\theta := 0.1$. The other parameters are defined as in Table 1.

Figure 3(C): Plots of $\rho_T(t)$ (solid line) and $\rho_C(t)$ (dashed line) for $t \in [0; t_f]$ with $t_f := 40$. Simulations are performed with $c_E(t) = c_P(t) = c_M(t) := 0$ for all $t \in [0; t_f]$, $\gamma := 0.018$ and $\theta := 0.001$. The other parameters are defined as in Table 1.

Figure 4: Plots of $n_T(t, v)$ (black) and $n_C(t, u)$ (grey) at time instants $t = 130$ (bottom panel), $t = 400$ (central panel) $t = 1000$ (top panel). Simulations are performed with $c_E(t) = c_P(t) = c_M(t) := 0$ for all $t \in [0; t_f]$, $\gamma := 0.1$ and $\theta := 0.01$. The other parameters are defined as in Table 1.

Figure 5(A): Plots of $\int_0^{0.01} n_T(t, v)\ dv$ (solid line) and $\int_0^{0.01} n_C(t, u)\ du$ (dashed line) for $t \in [0; t_f]$ with $t_f := 40$. Simulations are performed with $\gamma := 2.5$, $\theta := 0.1$ and $c_E(t) = c_P(t) = c_M(t) := 0$ for all $t \in [0; t_f]$. The other parameters are defined as in Table 1.

Figure 5(B): Plots of $\int_0^{0.01} n_T(t, v)\ dv$ (solid line) and $\int_0^{0.01} n_C(t, u)\ du$ (dashed line) for $t \in [0; t_f]$ with $t_f := 40$. Simulations are performed with $\gamma := 2.5$, $\theta := 0.1$, $c_E(t) := 4$ and $c_P(t) = c_M(t) := 0$ for all $t \in [0; t_f]$. The other parameters are defined as in Table 1.

Figure 5(C): Plots of $\int_0^{0.01} n_T(t, v)\ dv$ (solid line) and $\int_0^{0.01} n_C(t, u)\ du$ (dashed line) for $t \in [0; t_f]$ with $t_f := 40$. Simulations are performed with $\gamma := 2.5$, $\theta := 0.1$, $c_P(t) := 4$ and $c_E(t) = c_M(t) := 0$ for all $t \in [0; t_f]$. The other parameters are defined as in Table 1.

Figure 5(D): Plots of $\int_0^{0.01} n_T(t,v)\ dv$ (solid line) and $\int_0^{0.01} n_C(t,u)\ du$ (dashed line) for $t \in [0;t_f]$ with $t_f := 40$. Simulations are performed with $\gamma := 2.5$, $\theta := 0.1$, $c_M(t) := 4$ and $c_E(t) = c_P(t) := 0$ for all $t \in [0;t_f]$. The other parameters are defined as in Table 1.

Figure 6: Plots of $\frac{1}{t_f}\int_0^{t_f} \rho_T(t)\ dt$ (panel (A)) and $\frac{1}{t_f}\int_0^{t_f} \rho_C(t)\ dt$ (panel (B)), with $t_f := 360$, $\gamma := 1$ and $\theta := 0.001$, for increasing values of $\kappa(t_f)$. Simulations are performed with: $c_P(t) = c_M(t) := 0$ and $c_E(t) := c$ for all $t \in (0;t_f)$ (green line); $c_E(t) = c_M(t) := 0$ and $c_P(t) := c$ for all $t \in (0;t_f)$ (red line); $c_E(t) = c_P(t) := 0$ and $c_M(t) := c$ for all $t \in (0;t_f)$ (blue line); $c_E(t) = c_P(t) := c/2$ and $c_M(t) := 0$ for all $t \in (0;t_f)$ (yellow line); $c_E(t) = c_M(t) := c/2$ and $c_P(t) := 0$ for all $t \in (0;t_f)$ (cyan line); $c_P(t) = c_M(t) := c/2$ and $c_E(t) := 0$ for all $t \in (0;t_f)$ (pink line); $c_E(t) = c_P(t) = c_M(t) := c/3$ for all $t \in (0;t_f)$ (orange line). Different lines correspond to different values of the parameter c, which is tuned over the set $[0;48]$. In all cases, the other parameters are defined as in Table 1.

Figure S1(A)–(B): Plots of $1/t_f \int_0^{t_f} \rho_T(t)\ dt$ (Panel (A)) and $1/t_f \int_0^{t_f} \rho_C(t)\ dt$ (Panel (B)), with $t_f := 360$, $\gamma := 1$ and $\theta := 0.001$, for increasing values of $\kappa(t_f)$. Simulations are performed with: $c_E(t) := c\ \mathrm{sign}\left(\cos\left(2\pi t/15\right)\right)_+$ and $c_P(t) = c_M(t) := 0$ for all $t \in (0;t_f)$ (green line); $c_E(t) = c_M(t) := 0$ for all $t \in (0;t_f)$ and $c_P(t) := c\ \mathrm{sign}\left(\cos\left(2\pi t/15\right)\right)_+$ (red line); $c_M(t) := c\ \mathrm{sign}\left(\cos\left(2\pi t/15\right)\right)_+$ and $c_E(t) = c_P(t) := 0$ for all $t \in (0;t_f)$ (blue line); $c_M(t) := 0$ for all $t \in (0;t_f)$ and $c_E(t) = c_P(t) := c/2\ \mathrm{sign}\left(\cos\left(2\pi t/15\right)\right)_+$ (yellow line); $c_E(t) = c_M(t) := c/2\ \mathrm{sign}\left(\cos\left(2\pi t/15\right)\right)_+$ and $c_P(t) := 0$ for all $t \in (0;t_f)$ (cyan line); $c_E(t) := 0$ for all $t \in (0;t_f)$ and $c_P(t) = c_M(t) := c/2\ \mathrm{sign}\left(\cos\left(2\pi t/15\right)\right)_+$ (pink line); $c_E(t) = c_P(t) = c_M(t) := c/3\ \mathrm{sign}\left(\cos\left(2\pi t/15\right)\right)_+$ (orange line). Different lines correspond to different values of the parameter c, which is tuned over the set $[0;120]$. In all cases,

the other parameters are defined as in Table 1.

Figure S1(C)–(D): Plots of $1/t_f \int_0^{t_f} \rho_T(t)\ dt$ (Panel (C)) and $1/t_f \int_0^{t_f} \rho_C(t)\ dt$ (Panel (D)), with $t_f := 360$, $\gamma := 1$ and $\theta := 0.001$, for increasing values of $\kappa(t_f)$. Simulations are performed with: $c_P(t) = c_M(t) := 0$ for all $t \in (0; t_f)$ and $c_E(t) := c\,\mathrm{sign}\,(\cos(2\pi t/7))_+$ (green line); $c_P(t) := c\,\mathrm{sign}\,(\cos(2\pi t/7))_+$ and $c_E(t) = c_M(t) := 0$ for all $t \in (0; t_f)$ (red line); $c_E(t) = c_P(t) := 0$ for all $t \in (0; t_f)$ and $c_M(t) := c\,\mathrm{sign}\,(\cos(2\pi t/7))_+$ (blue line); $c_M(t) := 0$ for all $t \in (0; t_f)$ and $c_E(t) = c_P(t) := c/2\,\mathrm{sign}\,(\cos(2\pi t/7))_+$ (yellow line); $c_E(t) = c_M(t) := c/2\,\mathrm{sign}\,(\cos(2\pi t/7))_+$ and $c_P(t) := 0$ for all $t \in (0; t_f)$ (cyan line); $c_E(t) := 0$ for all $t \in (0; t_f)$ and $c_P(t) = c_M(t) := c/2\,\mathrm{sign}\,(\cos(2\pi t/7))_+$ (pink line); $c_E(t) = c_P(t) = c_M(t) := c/3\,\mathrm{sign}\,(\cos(2\pi t/7))_+$ (orange line). Different lines correspond to different values of the parameter c, which is tuned over the set $[0; 120]$. In all cases, the other parameters are defined as in Table 1.

Supplementary Figures

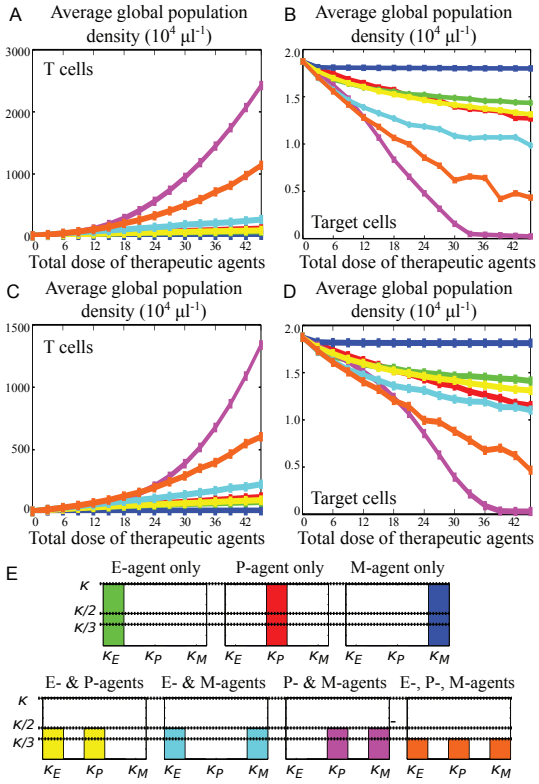

Figure S1. The most effective immunotherapy protocols rely on the simultaneous infusion of P-agents and M-agents. Panels (A)–(D): time-average of the global population density of T cells – Panels (A) and (C) – and target cells – Panels (B) and (D) – for increasing total doses of therapeutic agents κ (in units of 10^3 $pg/\mu l$). Different colours correspond to different therapeutic protocols that rely on the periodic infusion of E-agents/P-agents/M-agents separately and in combination (*i.e.*, different values of κ_E, κ_P and κ_M). Panels (A)–(B) and Panels (C)–(D) refer, respectively, to lower and higher infusion frequency. Panel (E): illustration of the protocols in use during the *in silico* experiments of Panels (A)–(D). Colours correspond to the plots shown in Panels (A)–(D). All therapeutic protocols under consideration lead to an increase in the time-average of the total number of T cells and a reduction in the time-average of the total number of target cells. However, when the infusion rates of therapeutic agents are sufficiently high, the protocols relying on the simultaneous infusion of sufficiently high concentrations of P-agents and M-agents lead to a larger population of T cells and to a significantly smaller population of target cells.

Analysis of the Mathematical Model

In order to verify the robustness of the conclusion presented in the main text – *i.e.,* the idea that protocols relying on the simultaneous infusion of P-agents and M-agents lead to a larger population of T cells – with respect to the choice of the model parameters, we perform a qualitative analysis of the global population density of T cells under the therapeutic protocols presented in Fig. 6(C). To this end, we define the sets

$$\mathcal{C}_1 := \left\{ \big(c,0,0\big), \big(0,c,0\big), \big(0,0,c\big) \right\},$$

$$\mathcal{C}_2 := \left\{ \Big(\frac{c}{2},\frac{c}{2},0\Big), \Big(\frac{c}{2},0,\frac{c}{2}\Big), \Big(0,\frac{c}{2},\frac{c}{2}\Big) \right\},$$

and

$$\mathcal{C}_3 := \left\{ \Big(\frac{c}{3},\frac{c}{3},\frac{c}{3}\Big) \right\}.$$

Furthermore, we define

$$\inf_{(u,v)\in[0;1]^2} g(u,v;\gamma,\theta) := \underline{g} > 0,$$

and we introduce the notation $\rho_T(t)\ |_{\mathbf{c}}$ to indicate the integral of the solution of equation (2) at the time t in the case where $c_E(t)$, $c_M(t)$ and $c_P(t)$ are defined, respectively, as the first, second and third component of the vector $\mathbf{c}(t)$, that is,

$$\mathbf{c}(t) := \big(c_E(t), c_M(t), c_P(t)\big).$$

In the framework of the above definitions and notations, we can prove the following

Lemma 1.1 *Let*

$$\mathbf{c}(t) := \mathbf{c} = (c_E, c_M, c_P) \in \mathcal{C}_1 \cup \mathcal{C}_2 \cup \mathcal{C}_3 \quad \textit{for all } t \geq 0, \tag{7}$$

and assume

$$0 < \rho_C(t=0) \leq \frac{\alpha_C}{\mu_C} \quad \textit{and} \quad 0 < \rho_T(t=0) \leq \Big[\beta_T(1+c_E)\rho_C(t=0)+\alpha_T(1+c_P)\Big]\frac{(1+c_M)}{\mu_T}. \tag{8}$$

Then, the following a priori estimates hold:

$$0 \leq \rho_C(t) \leq \frac{\alpha_C}{\mu_C} \quad \textit{and} \quad 0 < \rho_T(t) \leq \Big[\beta_T(1+c_E)\frac{\alpha_C}{\mu_C}+\alpha_T(1+c_P)\Big]\frac{(1+c_M)}{\mu_T}, \tag{9}$$

for all $t \geq 0$. *Furthermore, there exists* $0 < t^* < \infty$ *such that*

$$\rho_T(t) \geq \frac{\alpha_T}{\mu_T}(1+c_P)(1+c_M) \qquad \textit{for any } \; t > t^*. \tag{10}$$

Proof 1.1 *The non-negativity of the functions* n_C *and* n_T *can be proved in a similar way as that presented, for instance, in [1]; therefore, we leave the first and second lower bounds of* (9) *without proof. On the other hand, to prove the first upper bound of* (9), *we integrate equation* (1) *over the set* $[0;1]$, *and we use definition* (3) *together with the non-negativity of the functions* n_C *and* n_T *to obtain*

$$\frac{d}{dt}\rho_C(t) \leq \big(\alpha_C - \mu_C\, \rho_C(t)\big)\, \rho_C(t).$$

Under the first assumptions of (8), *the above differential inequality implies the first upper bound of* (9). *In order to prove the second upper bound of* (9), *we integrate equation* (2) *over the set* $[0;1]$, *and we make use of definition* (4) *and the non-negativity of the functions*

n_C and n_T to achieve

$$\begin{aligned}\frac{d}{dt}\rho_T(t) &\leq (1+c_E)\,\beta_T\,\rho_C(t)\,\rho_T(t)\\ &+ (1+c_P)\,\alpha_T\,\rho_T(t)\\ &- \frac{\mu_T}{1+c_M}\,\rho_T(t)\,\rho_T(t). \qquad (11)\end{aligned}$$

Under the second assumptions of (8)*, the above differential inequality together with the first upper bound of* (9) *imply the second upper bound of* (9)*. In the same way, we can see that*

$$\frac{d}{dt}\rho_T(t) \geq (1+c_P)\,\alpha_T\,\rho_T(t) - \frac{\mu_T}{1+c_M}\,\rho_T(t)\,\rho_T(t);$$

that way we achieve the lower bound (10) *and then conclude the proof.*

Lemma 1.1 allows us to prove the following:

Theorem 1.2 *Let the assumptions of Lemma 1 hold. Then, there exist a threshold value of the infusion rate $K < \infty$, and a threshold value of the exposure time $\tau < \infty$ such that, if $c > K$,*

$$\underset{c\in\mathcal{C}_1\cup\mathcal{C}_2\cup\mathcal{C}_3}{\arg\max}\ \rho_T(t)\,|_{\mathbf{c}} = \left(0, \frac{c}{2}, \frac{c}{2}\right) \quad \textit{for all } t > \tau. \qquad (12)$$

Proof 1.2 *We begin by defining the function*

$$\lambda(t) := \rho_C(t)\,\frac{\beta_T}{\alpha_T},$$

and we show that, for c sufficiently large, there exists $0 < t_* < \infty$ such that $\lambda(t) \leq 0.5$ for all $t > t_*$. In fact, equation (2) *implies that*

$$\frac{d}{dt}\rho_T(t) \geq \Big[\beta_T\,\underline{g}\,(1+c_E)\rho_C(t) + \alpha_T(1+c_P) - \frac{\mu_T}{1+c_M}\rho_T(t)\Big]\rho_T(t),$$

and so there exists $0 < t_* < \infty$ *such that*

$$\rho_T(t) \geq \frac{\beta_T}{\mu_T}\, \underline{g}\, (1+c_E)\, (1+c_M)\rho_C(t) + \frac{\alpha_T}{\mu_T}(1+c_P)\, (1+c_M)$$

for all $t > t_*$. *In turn, using the above inequality in equation* (1), *we obtain*

$$\begin{aligned}\frac{d}{dt}\rho_C(t) \leq & \Big[\alpha_C - \mu_C\rho_C(t)\Big]\rho_C(t) \\ & - \Big[\beta_C\, \underline{g}^2\, \frac{\beta_T}{\mu_T}\, (1+c_E)\, (1+c_M)\rho_C(t)\Big]\rho_C(t) \\ & - \beta_C\, \underline{g}\, \frac{\alpha_T}{\mu_T}\, (1+c_P)\, (1+c_M)\rho_C(t),\end{aligned}$$

which implies

$$\rho_C(t) \leq \frac{\alpha_C - \beta_C\, \underline{g}\, \alpha_T/\mu_T\, (1+c_P)\, (1+c_M)}{\mu_C + \beta_C\, \underline{g}^2\, \beta_T/\mu_T\, (1+c_E)\, (1+c_M)},$$

for any $t > t_*$. *Under assumption* (7), *the above inequality allows us to conclude that there exists* $0 < c_* < \infty$ *such that if* $c > c_*$ *then* $\lambda(t) \leq 0.5$ *for all* $t > t_*$.

Moreover, under assumption (7), *the differential inequality* (11) *implies the following inequalities:*

$$\rho_T(t)\,|_{\mathbf{c}=(c,0,0)} \leq \frac{\alpha_T}{\mu_T}\big[1+\lambda(t)\big(1+c\big)\big] \qquad \textit{(E-agent only)}, \tag{13}$$

$$\rho_T(t)\,|_{\mathbf{c}=(0,c,0)} \leq \frac{\alpha_T}{\mu_T}\big[1+\lambda(t)\big]\big(1+c\big) \qquad \textit{(M-agent only)}, \tag{14}$$

$$\rho_T(t)\,|_{\mathbf{c}=(0,0,c)} \leq \frac{\alpha_T}{\mu_T}\big[\big(1+c\big)+\lambda(t)\big] \qquad \textit{(P-agent only)}, \tag{15}$$

$$\rho_T(t)\,|_{\mathbf{c}=(c/2,c/2,0)} \leq \frac{\alpha_T}{\mu_T}\Big[\Big(1+\frac{c}{2}\Big)+\lambda(t)\Big(1+\frac{c}{2}\Big)^2\Big] \qquad \textit{(E- \& M-agents)}, \tag{16}$$

$$\rho_T(t)\,|_{\mathbf{c}=(c/2,0,c/2)} \leq \frac{\alpha_T}{\mu_T}\Big[\Big(1+\frac{c}{2}\Big)+\lambda(t)\Big(1+\frac{c}{2}\Big)\Big] \qquad \textit{(E- \& P-agents)}, \tag{17}$$

$$\rho_T(t)\mid_{\mathbf{c}=(c/3,c/3,c/3)} \leq \frac{\alpha_T}{\mu_T}\Big[\Big(1+\frac{c}{3}\Big)^2+\lambda(t)\Big(1+\frac{c}{3}\Big)^2\Big] \qquad \textit{(E-, M- \& P-agents)}, \tag{18}$$

for all $t>0$. *On the other hand, the lower bound* (10) *implies that, for any* $t>t^*$,

$$\rho_T(t)\mid_{\mathbf{c}=(0,c/2,c/2)} \geq \frac{\alpha_T}{\mu_T}\Big(1+\frac{c}{2}\Big)^2 \qquad \textit{(M- \& P-agents)}. \tag{19}$$

Since $\lambda(t)\leq 0.5$ *for any* $t>t_*$, *we can conclude that there exists* $0<c^*<\infty$ *such that the right hand side of inequality* (19) *is larger than the right hand sides of inequalities* (13)-(18) *for all* $t>t_*$. *A graphical representation of this result is provided in Fig. S2. This figure shows the ratio between the right hand side of inequality* (19) *and the right hand sides of each one of the six inequalities* (13)-(18) *for different values of* λ *and* c.

In conclusion, defining $\tau:=\max(t_*,t^*)$ *and* $K:=\max(c_*,c^*)$, *we obtain identity* (12).

References

1. Perthame, B. 2007. *Transport Equations in Biology.* Birkhäuser, Basel.

2. Lorz, A., Lorenzi, T., Hochberg, M.E., Clairambault, J., and Perthame, B. Populational adaptive evolution, chemotherapeutic resistance and multiple anti-cancer therapies *ESAIM-Math Model Num* 2013; 47:377–399.

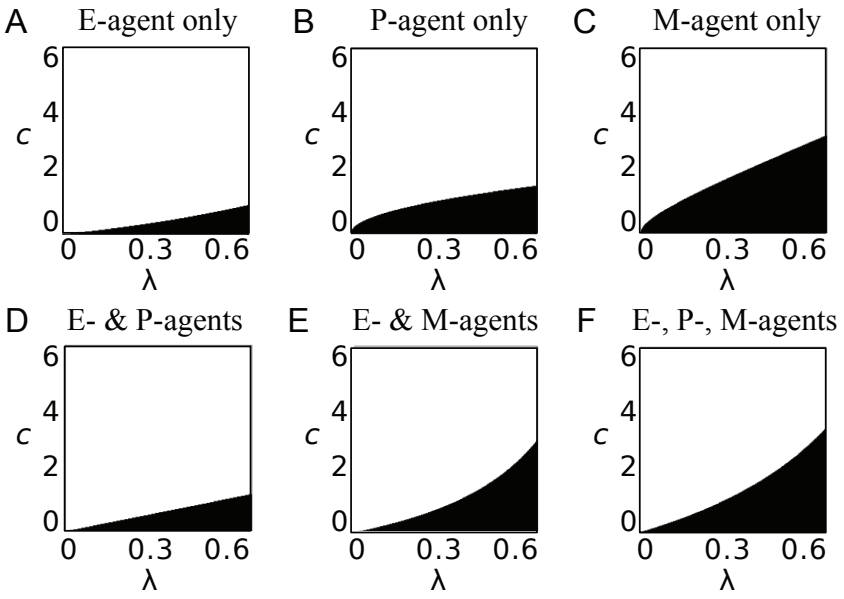

Figure S2. Graphical representation of the result established by Theorem 1.2. Ratio between the right hand side of inequality (19) and the right hand sides of inequalities (13)-(18), according to the values of λ and c. The white regions indicate the range of values of λ and c where the right hand side of inequality (19) is larger than the right hand side of one of the six inequalities (13)-(18) (indicated by the heading of the panel).